



<http://www.diva-portal.org>

This is the published version of a paper published in *Annals of Nuclear Energy*.

Citation for the original published paper (version of record):

Chen, Y., Zhang, H., Ma, W. (2022)

Coupled MELCOR/COCOMO analysis on quench of ex-vessel debris beds

*Annals of Nuclear Energy*, 165: 108643

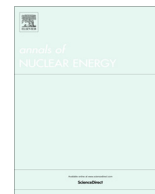
<https://doi.org/10.1016/j.anucene.2021.108643>

Access to the published version may require subscription.

N.B. When citing this work, cite the original published paper.

Permanent link to this version:

<http://urn.kb.se/resolve?urn=urn:nbn:se:kth:diva-300765>



# Coupled MELCOR/COCOMO analysis on quench of ex-vessel debris beds

Yangli Chen, Huimin Zhang, Weimin Ma\*

Royal Institute of Technology (KTH), Roslagstullsbacken 21, 106 91 Stockholm, Sweden

## ARTICLE INFO

### Article history:

Received 30 March 2021

Received in revised form 9 August 2021

Accepted 13 August 2021

### Keywords:

Severe accident  
Debris bed coolability  
Coupled analysis  
MELCOR  
COCOMO

## ABSTRACT

The cornerstone of severe accident strategy of Nordic BWRs is to flood the reactor cavity for the long-term coolability of an ex-vessel debris bed. As a prerequisite of the long-term coolability, the hot debris bed formed from fuel coolant interactions (FCI) should be quenched. In the present study, coupling of the MELCOR and COCOMO codes is realized with the aim to analyze the quench process of an ex-vessel debris bed under prototypical condition of a Nordic BWR. In this coupled simulation, MELCOR performs an integral analysis of accident progression, and COCOMO performs the thermal-hydraulic analysis of the debris bed in the flooded cavity. The effective diameter of the particles is investigated. The discussion on the bed's shape shows a significant effect on the propagation of the quench front, due to different flow patterns. Compared with MELCOR standalone simulation, the coupled simulation predicts earlier cavity pool saturation and containment venting.

© 2021 The Authors. Published by Elsevier Ltd. This is an open access article under the CC BY license (<http://creativecommons.org/licenses/by/4.0/>).

## 1. Introduction

During a severe accident of the light water reactor, the reactor core would gradually heat up, degrade and relocate into the lower plenum of the vessel. The corium would be discharged to the cavity when the lower head failure occurs. The severe accident strategy employed by Nordic BWR is to flood the cavity into a deep water pool. The discharged corium melt from the vessel would breakup and fragment into small particles in the cavity pool, and subsequently form a particulate debris bed on the cavity floor. The ultimate goal of the severe accident strategy is to remove the residual decay power for a long time, in order to stabilize the accident progression and avoid further debris heat-up and even re-melting.

The coolability of debris beds during severe accidents has attracted much attention in the past decades. Investigations have been performed for coolability of the debris bed formed inside the vessel lower plenum (Huang and Ma, 2019a; Yakush et al., 2014; Yakush et al., 2013; Yakush and Kudinov, 2016), and inside the cavity pool (Chen and Ma, 2020; Huang and Ma, 2018a). The “dryout” heat flux or power density, considered as the debris bed maximum capability for the decay removal, has received extensive studies both on experiment and model development (Hu and Theofanous, 1991; Lipinski, 1982; Thakre et al., 2014). However, these studies normally assume the initial condition as a thermal equilibrium state between the debris bed and the saturated water pool. However, the quench process, which is the prerequisite to

reach the thermal equilibrium state, lacks the attention. When the debris bed is formed, the initial high temperature difference between the debris bed and the coolant leads to intense boiling on the particle surface, and the inner porous zones of the bed would be dry by the intense evaporation. Before the water quenches the local dry zones inside the debris bed, the thermal equilibrium may not exist locally. Then the temperature of the dry particles would continuously increase due to the decay power. It is essential to know how the quench front propagates in the debris bed, and whether the hot and dry zones inside the bed could be quenched before re-melting.

During the debris bed quench process, the large temperature difference between solid particles and water, and the complex two-phase flow pattern bring difficulties for experimental measurement and modelling. Several experiments on the quench of hot particle bed with either top or bottom flooding have provided valuable observations (Cho et al., 1984; Tung and Dhir, 1987; Tutu et al., 1984). More recently, the DEBRIS facility investigated the quench of hot and dry debris bed in a cylindrical test section with induction heating. The tests compared both top and bottom inflow conditions for the reflooding of the hot and dry debris beds, and characterized the total quenching time (Schäfer et al., 2006). The PEARL facility was featured with the large bed scale and the presence of a lateral bypass at the periphery. The tests provided insights of debris bed quench, and valuable data for model development and validation (Chikhi and Fichot, 2017).

Analytical or empirical correlations were proposed based on experimental observations and simplified assumptions (Chikhi and Fichot, 2017; Tung and Dhir, 1987; Tutu et al., 1984). These

\* Corresponding author.

E-mail addresses: [yanglic@kth.se](mailto:yanglic@kth.se) (Y. Chen), [weimin@kth.se](mailto:weimin@kth.se) (W. Ma).

**Nomenclature**

$c_p$	isobaric specific heat [J/(kg·K)]	$\varepsilon$	porosity
$D$	Diameter (m)	$\mu$	dynamic viscosity [kg/(m·s)]
$e$	specific internal energy (J/kg)	$\rho$	density (kg/m <sup>3</sup> )
$g$	gravitational acceleration constant (m/s <sup>2</sup> )	$\sigma$	surface tension (N/m)
$h_{fg}$	latent heat of vaporization (J/kg)	<b>Subscripts</b>	
$h$	heat transfer coefficient [W/(m <sup>2</sup> ·K)]	$b$	bubble
$i$	specific enthalpy (J/kg)	$g$	gas
$Ja$	Jakob number	$l$	liquid
$k$	conductivity [W/(m·K)]	$max$	maximum
$K$	friction coefficient	$min$	minimum
$L$	thickness of the bed (m)	$p$	particle
$Nu$	Nusselt number	$rel$	relative
$p$	pressure (Pa)	$s$	solid
$Pr$	Prandtl number	$sat$	saturation
$Q$	heat flux (W/m <sup>2</sup> )	<b>Superscripts</b>	
$Re$	Reynolds number	$B$	bubbly flow
$s$	saturation	$D$	droplet flow
$T$	temperature (K)	$evap$	evaporation
$t$	time (s)	$FB$	Film boiling
$v$	velocity	$PB$	pool boiling
$W$	weight function	$trans$	transition
<b>Greek letters</b>			
$\Gamma$	mass transfer rate [kg/(m <sup>3</sup> ·s)]		

correlations are one-dimensional, which focus on merely global parameters, e.g. the steam flow rate or the quench front velocity. To obtain more details e.g. the flow field, local temperature transient etc., the numerical codes are needed to perform the multi-dimensional simulation. COCOMO code by IKE University of Stuttgart is developed with the specific aim to solve the boiling heat transfer of particulate debris bed in reactors. It is capable to perform the numerical simulation for debris bed quench and long-term coolability. Extensive studies have performed to systematically validate the COCOMO code with DEBRIS, PEARL, COOLOCE, and POMECO experiments (Bürger et al., 2006; Huang and Ma, 2018a; Huang and Ma, 2018b; Takasuo et al., 2012). In the present study, the COCOMO code is used to perform the numerical simulation for the quench process of the prototypical ex-vessel debris bed, for the safety analysis of the severe accident strategy of Nordic BWR.

The prototypical ex-vessel debris bed is related to the severe accident progression. For instance, the in-vessel accident progression could affect the amount and the temperature of the melt when it releases to cavity, and vessel failure time could affect the decay power of the ex-vessel debris bed. In order to acquire a reliable scenario of the prototypical ex-vessel debris bed, a MELCOR/COCOMO coupling interface is developed in the present study. Due to the lumped-parameter feature of the MELCOR code, the models implemented in MELCOR is normally parametric and empirical. Many researchers have developed the coupled simulation of MELCOR with other codes to extend the MELCOR capability and acquire more local details. For instance, MELCOR has been coupled with other codes such as GASFLOW for hydrogen distribution in containment (Szabó et al., 2014), REALAP5 for modeling the thermosiphon loop (Huang and Ma, 2019a), and PECM model in OpenFOAM for molten core material in the lower head (Dietrich, 2016).

This paper is organized as follows. Section 2 introduces the MELCOR and COCOMO code, specifically the comparison of CAV package of MELCOR with COCOMO code. Section 3 shows the development of the coupling interface for MELCOR/COCOMO. Sec-

tion 4 presents the results and discussions on the coupled simulation applied on Nordic BWR. Section 5 draws the conclusion.

## 2. Simulation codes

MELCOR, as an integral system code for the severe accident simulation, contains the model to simulate the ex-vessel corium behavior. However, the model implemented in MELCOR is not applicable for the particulate debris bed, which is expected to form in the deep cavity pool of Nordic BWR during severe accident. This section provides a brief comparison of the models implemented in MELCOR and COCOMO code, in order to illustrate the motivation to develop the coupled simulation.

### 2.1. MELCOR models

The MELCOR simulation of the severe accident of a light water reactor is achieved by the cooperation of packages implemented in the MELCOR code. Each package models a specific portion of the accident phenomena or program control. The behavior of the corium in the cavity is modelled with the Cavity (CAV) package, including the effect of heat transfer, concrete ablation, cavity shape change, gas generation, and debris/gas chemistry. The CAV package considers an axisymmetric system of the concrete cavity retaining corium in one or several layers, as depicted in Fig. 1. Once the corium is deposited in the CAV package, it is assumed to cover the entire area of the cavity floor instantaneously.

For energy conservation, the corium layer is treated in a lumped way that each layer is averaged with one temperature. Thus, it is a one-dimensional system for heat transfer. There is conduction or natural convection models to calculate the heat transfer between the interfaces. A bounding control volume is used as the boundary condition for the top surface of the corium. It means that the cooling process of the corium by the pool only occurs on the top surface. An implemented pool boiling curve is used to calculate the

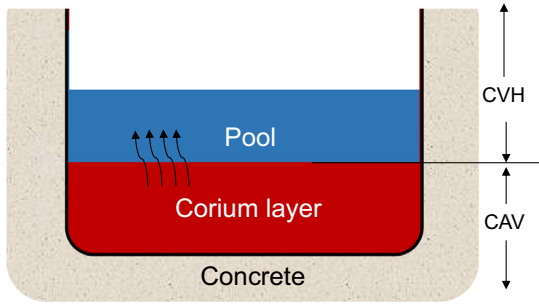


Fig. 1. Schematic of MELCOR CAV package model.

heat loss. Then, the continuity of the heat flux determines the temperature of the corium layers.

## 2.2. Numerical models of COCOMO code

COCOMO code is developed by IKE, University of Stuttgart (Bürger et al., 2006). It has the capability to simulate the boiling-off and multi-phase flow during the cooling process of a hot particulate debris bed in the lower head or in the reactor cavity, during a severe accident. As a numerical code, it solves the conservation equations for three phases separately, including particles in solid phase and coolant in liquid and gas phase. The non-equilibrium interactions between phases are considered.

Extensive validation works against experiments have confirmed the capability of the COCOMO simulation on quench process of hot particle beds. Early validation studies have been performed against the bottom-flooding quenching experiment of Tutu et al. (1984), with the concern on temperature development and heat flux at bed top (Bürger et al., 2006). The validation against DEBRIS experiment showed good agreement on the quench front propagation for top-flooding experiment (Schäfer et al., 2006). A recent validation work has been performed against PEARL experiment, which features a large scale quench process of hot particles with the presence of a bypass. Results showed good agreement in terms of several key parameters, such as velocity of the quench front and production rate of steam (Huang and Ma, 2018b).

### 2.2.1. Momentum equations

The particulate debris bed is treated as a fixed matrix of high-permeability porous medium with user-defined porosity and particle size, and coolant can ingress into the porous zones. It is assumed that the dominating forces for the coolant fluids flowing in the porous medium are (i) the friction forces between fluids and solid particles; (ii) the interfacial drag between liquid and gas phase; (iii) pressure gradient; and (iv) buoyancy force. The momentum conservation equations for the coolant fluids are simplified by neglecting the inertial terms of the temporal and spatial derivatives of the velocity, and considering only four dominating forces in Eqs. (1) and (2).

$$K_{gs} \vec{v}_g + \frac{K_{gl}}{(1-s)} (\vec{v}_g - \vec{v}_l) = -\nabla p_g + \rho_g \vec{g} \quad (1)$$

$$K_{ls} \vec{v}_l + \frac{K_{gl}}{s} (\vec{v}_g - \vec{v}_l) = -\nabla p_l + \rho_l \vec{g} \quad (2)$$

In the equations from the left to the right, four terms represent the four dominating forces mentioned above. For the friction coefficient ( $K_{gs}$ ,  $K_{ls}$ ) and the interfacial drag coefficient  $K_{gl}$ , several empirical models are implemented in the COCOMO code, including (i) Lipinski mode (Lipinski, 1982), (ii) Reed model (Reed, 1982), (iii) Hu & Theofanous model (Hu and Theofanous, 1991), (iv) Schulenberg & Müller model (Schulenberg and Müller, 1986), (v) Tung & Dhir model (Tung and Dhir, 1988), and (vi) modified Tung & Dhir model. The first three models are developed from Ergun's equation (Ergun, 1952), which is the single-phase friction law in the porous medium. The Ergun's equation is extended into two-phase by introducing relative permeability and passability, with different forms. The detailed forms of the model can be found in our previous studies (Huang and Ma, 2018a; Huang and Ma, 2018b). The validation of these two-phase friction models implemented in the COCOMO code were performed with experiments by the POMECO-FL facility, of which the result shows that the Reed model has the best agreement. (Huang and Ma, 2018b). Thus, the Reed model is used in the present study for the friction coefficients.

### 2.2.2. Energy equations

The energy equations for coolant in gas phase and liquid phase, and for particles in solid phase are listed in the following equations (3)–(5), respectively.

$$\begin{aligned} \frac{\partial}{\partial t} \varepsilon(1-s)\rho_g e_g + \nabla \cdot (\varepsilon(1-s)\rho_g \vec{v}_g i_g) \\ = \nabla \cdot (k_g \nabla T_g) + Q_{s,g} - Q_{g,sat} + \Gamma^{evap} i_{g,sat} \end{aligned} \quad (3)$$

$$\frac{\partial}{\partial t} \varepsilon s \rho_l e_l + \nabla \cdot (\varepsilon s \rho_l \vec{v}_l i_l) = \nabla \cdot (k_l \nabla T_l) + Q_{s,l} - Q_{l,sat} - \Gamma^{evap} i_{l,sat} \quad (4)$$

$$\frac{\partial}{\partial t} \rho_s e_s = \nabla \cdot (k_s \nabla T_s) + Q_s^{Decay} - Q_{s,g} - Q_{s,l} \quad (5)$$

The heat transfers from solid particles to the liquid, gas and interface are considered separately with conditions listed in Table 1. For the boiling heat transfer of solid particles, a minimum film boiling temperature is defined as  $T_{min}^{FB} = T_{sat} + 17K$ , and a maximum pool boiling temperature is defined as  $T_{max}^{PB} = T_{min}^{FB} + 100K$ . When solid temperature is below  $T_{min}^{FB}$ , pool boiling is assumed. When solid temperature is above  $T_{max}^{PB}$ , pure film boiling is assumed. In the transient zone, the heat transfer coefficient is obtained by linear interpolation.

Table 1

Heat transfer correlations.

Heat flux	Correlations
$Q_{s,l}$	Satisfy both: (i) $T_s < T_{sat}$ ; (ii) liquid is continuous $Nu_{s,l} = 2 + 0.6Re_l^{1/2} Pr_l^{1/3}$
$Q_{s,g}$	Satisfy both: (i) $T_s > T_{sat}$ ; (ii) gas is continuous $Nu_{s,g} = 2 + 0.6Re_g^{1/2} Pr_l^{1/3}$
$Q_{s,sat}$	Pool boiling $T_s \leq T_{min}^{FB}$ : $T_{min}^{FB} = T_{sat} + 17K$ $h_{s,sat}^{PB} = \frac{c_{p,l} \cdot \mu_l \cdot (T_s - T_{sat})^2}{(i_{g,sat} - i_{l,sat})^2 \cdot (0.012 Pr_l)^3 \cdot \sqrt{g(\rho_l - \rho_g)}}$ Film boiling $T_s \geq T_{max}^{PB}$ : $T_{max}^{PB} = T_{min}^{FB} + 100K$ $Nu_{s,sat}^{FB} = 0.67 \cdot \left( \frac{\rho_g \cdot g \cdot (\rho_l - \rho_g) \cdot \Delta i'_{sat} \cdot D_p^3}{\mu_g \cdot k_g \cdot (T_s - T_{sat})} \right)^{1/4}$ where modified latent heat $\Delta i'_{sat} = (i_{g,sat} - i_{l,sat}) \cdot \left[ 1 + \left( \frac{0.163}{Pr_g} \right) \cdot Ja \right] Ja = \frac{c_{p,g} \cdot (T_s - T_{sat})}{i_{g,sat} - i_{l,sat}}$ Transition region $T_{min}^{FB} < T_s < T_{max}^{PB}$ : $h_{s,sat}^{trans} = [1 - W(T_s)] \cdot h_{s,sat}^{PB} + W(T_s) \cdot h_{s,sat}^{FB}$ $W(T_s) = \frac{T_s - T_{min}^{FB}}{T_{max}^{PB} - T_{min}^{FB}}$
$Q_{l,sat}$	Bubbly flow: $Nu_{l,sat}^B = 2 + 0.6Re_{l,rel}^{1/2} Pr_l^{1/3}$ Droplet flow: $Nu_{l,sat}^D = 10$
$Q_{g,sat}$	Bubbly flow: $Nu_{g,sat}^B = 10$ Droplet flow: $Nu_{g,sat}^D = 2 + 0.738Re_{g,rel}^{1/2} Pr_g^{1/3}$

As for the heat transfer between interface and liquid or gas bulk, the two-phase flow is separated into three regimes based on the liquid fraction, denoted by  $s$ . As default: when  $s > 0.7$ : liquid phase is the continuous field and in bubbly flow; when  $s < 0.3$ : gas phase is the continuous field and in droplet flow; when  $0.3 < s < 0.7$ : bubbly flow and droplet co-exist, and it is weighted by the liquid fraction. The diameters of bubbles  $D_b$ , droplets  $D_d$  and solid particles  $D_p$  are assumed with the relationship:  $D_b = D_d = 0.125D_p$ .

### 3. Coupling of MELCOR and COCOMO

Due to the absent capability of MELCOR to model the ex-vessel cooling of particulate debris bed, this paper intends to develop a coupled simulation to extend the MELCOR capability. The coupled simulation adopts COCOMO code to simulate the thermal hydraulics of the debris bed, and MELCOR code to perform the integral simulation of the severe accident progression.

As illustrated in Fig. 2, the left part shows the MELCOR nodalization of the containment of a reference Nordic BWR. The lower drywell is flooded into a deep water pool during a postulated severe accident, where the released molten corium from the vessel would form a debris bed. The right part of the figure shows the computational domain of the COCOMO simulation, which is the pool region in the lower drywell. After vessel failure is predicted in MELCOR, the coupling interface is activated and COCOMO start to simulate the debris bed cooling as a substitution of CAV package of MELCOR. The Fuel Dispersal Interactions (FDI) package of MELCOR is activated to calculate the energy transfer from corium to the pool during settling process, with a parametric model. In order to avoid the CAV calculation in MELCOR in the coupled simulation, a zero translation matrix for the mass transfer from COR package to CAV package is used to vanish the corium mass once it is released from the vessel. The coupled simulation exchanges information between two codes. MELCOR sends the pressure and the pool temperature to COCOMO as the initial and boundary conditions, and also sends decay power as the heat source of the debris bed. COCOMO sends the heat transfer rate to MELCOR as the energy source of the pool for calculation of the thermal-hydraulic response in the containment.

The coupled simulation framework requires four modules, as shown in Fig. 3. Other than MELCOR and COCOMO code, there is a communication program MPIEXEC and an external coupling program DINAMO. MPIEXEC is a MPI based coupling interface for MELCOR, developed by Sandia National Laboratories (Young et al., 2004). It controls the execution of the coupled codes and coordinates the data exchange. DINAMO (Direct Interface for Adding Models) is developed by KIT, with the specific aim to couple new

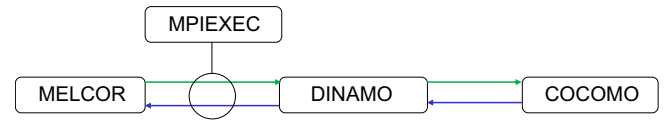


Fig. 3. The coupling framework of MELCOR/COCOMO.

models to MELCOR code (Dietrich, 2016). It consists of two major functions: (i) the coupling routines which enable the communication with MELCOR via the MPIEXEC program, and (ii) an interface which allows for the integration of new models into the source code as well as an easy communication with external programs. The development of the coupled simulation framework of MELCOR/COCOMO is achieved by integrating the DINAMO source code with the COCOMO source code together. A new executable is compiled, containing both the coupling interface and the COCOMO code. Therefore, the data exchange from the coupling interface to the COCOMO side could be accomplished internally and fast, rather than via external files.

The synchronization logic for data exchange between two codes is shown in Fig. 4. Two horizontal time axes represent the advancement of the calculation process for MELCOR and COCOMO, in green and blue respectively. The interval of the time axes indicates the length of the time step for each advancement. The number above the green axis or below the blue axis denotes the order of the advancing steps during the coupling calculation. MELCOR first starts the simulation of the severe accident progression of a reactor from scram. After MELCOR predicts the vessel failure, data from MELCOR is sent to COCOMO for initialization. MELCOR runs for one timestep with time interval  $\Delta t_1$ , and it suspends at the end of this timestep. The coupling interface sends the time interval  $\Delta t_1$  to COCOMO and triggers the start of COCOMO simulation. COCOMO code runs several timesteps (e.g.  $\Delta t_2 \sim \Delta t_5$  in the figure), until COCOMO and MELCOR meet at the same time point. Two codes then exchange data at this time point, which is the end of  $\Delta t_1$  for MELCOR and at the end of  $\Delta t_5$  for COCOMO. Then the coupled simulation proceeds for the next cycle.

### 4. Application and discussion

The coupled simulation is applied to a reference Nordic BWR with a hypothetical station blackout (SBO) scenario (Chen et al., 2019). The reference Nordic BWR has the thermal power of 3900 MW during normal operation. The lower drywell is a cylindrical chamber with a radius of 6.1 m, as shown in the left part of Fig. 2. As a severe accident mitigation strategy, the lower drywell

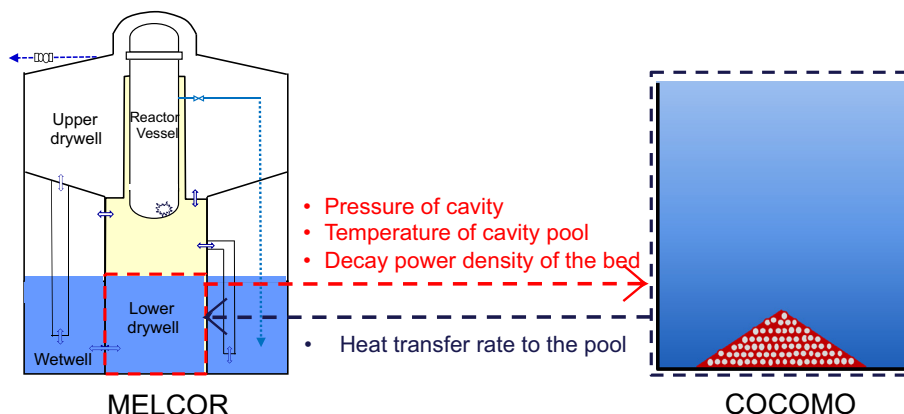


Fig. 2. MELCOR/COCOMO coupled simulation and data exchange.

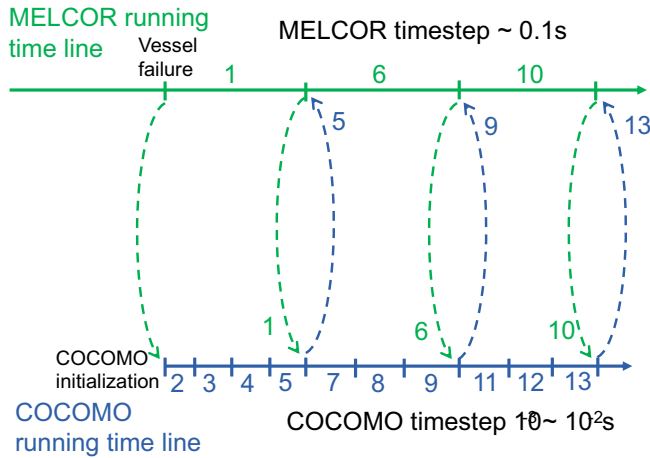


Fig. 4. Synchronization logic for data exchange.

is flooded after SBO, with subcooled water from the surrounding lower wetwell, in order to cool the released molten corium from the vessel. The water pool depth is around 7 m. A study shows that if a thin melt jet (e.g. jet diameter 10 ~ 20 cm) is released into a deep water pool (e.g. depth > 5 m), a significant breakup of the melt and formation of debris bed is expected (Rahman, 2013). In the present study, it is assumed all molten corium well-fragmented in the pool of lower drywell, and a debris bed formed on the floor.

#### 4.1. MELCOR standalone simulation

The MELCOR standalone simulation was first carried out, in order to obtain the released corium mass and composition for defining the debris bed in COCOMO code, and to compare with the coupled simulation. The standalone simulation predicts that the vessel failure occurs at approximately 6.0 h after reactor scram. The temperature and the mass of the debris calculated from the MELCOR CAV package are plotted in Fig. 5. It can be found that the corium release from the vessel is quite fast due to the gross failure of the lower head, with 298ton corium relocated in the cavity in around 30 min. The composition of the debris is listed in Table 2. Due to the one-layer assumption in the CAV package, the entire debris has the same temperature. The temperature decreases fast during the corium relocation period, and it gradually slows down. MELCOR predicts that the debris layer is still at high temperature above 1000 K at 20 h after vessel failure.

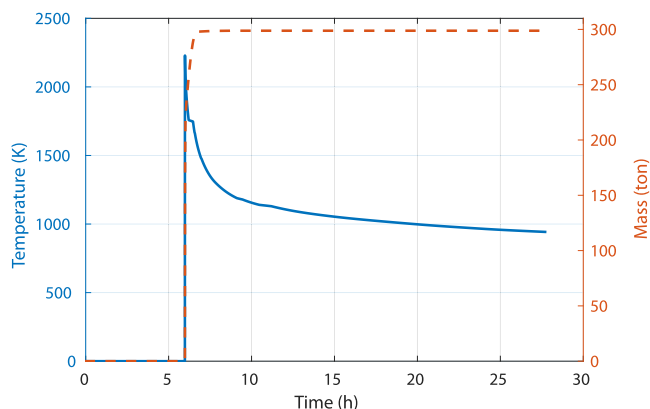


Fig. 5. MELCOR predictions of the corium temperature and mass in CAV.

Table 2

MELCOR predictions of the corium composition in CAV.

Composition	Mass percentage
UO <sub>2</sub>	48.9%
Zr	12.1%
ZrO <sub>2</sub>	4.9%
Stainless steel	33.1%

#### 4.2. MELCOR/COCOMO coupled simulation

##### 4.2.1. Simulation settings

In the coupled simulation, the computational domain of COCOMO code is in an axisymmetric coordinate as shown in Fig. 6. It covers the entire pool region of the cavity. The upper boundary is an open boundary set with the containment pressure as a variance of time, provided by MELCOR. The initial pool temperature is set as 324 K, which is the cavity pool temperature at vessel failure time provided by MELCOR.

The red region of Fig. 6 shows an example of debris bed defined with a conical shape. The debris bed has total mass of 298 tons. The debris is treated as a mixture of materials with specific mass percentages as listed in Table 2. The density of the mixture is calculated as the average density of all materials weighted by their mass percentages. Thermal properties such as heat capacity and thermal conductivity for each material are as functions of temperature. For the thermal properties of the mixture, they are calculated as the weighted average of the functions based on the mass percentages of the materials. The density and thermal properties of each material are from (Humphries et al., 2017). The oxidation of metal material is not considered. The debris particles are assumed to remain solid phase in current calculations. The remelting of the debris and the further melt infiltration in the debris bed is the consequent phenomena if the debris bed could not be cooled, which may influence the molten core concrete interaction (MCCI) and the integrity of containment. The modelling of remelting and melt infiltration is being investigated in other researches (Mohsen Hoseyni et al., 2021) and it is out of the scope of present study.

The decay power of the debris bed defined in COCOMO is provided by MELCOR simulation. In MELCOR, a normalized decay power curve for BWR is implemented and used in current study. The total decay power of Nordic BWR and the decay power of the debris bed in cavity are plotted as a variance of time after

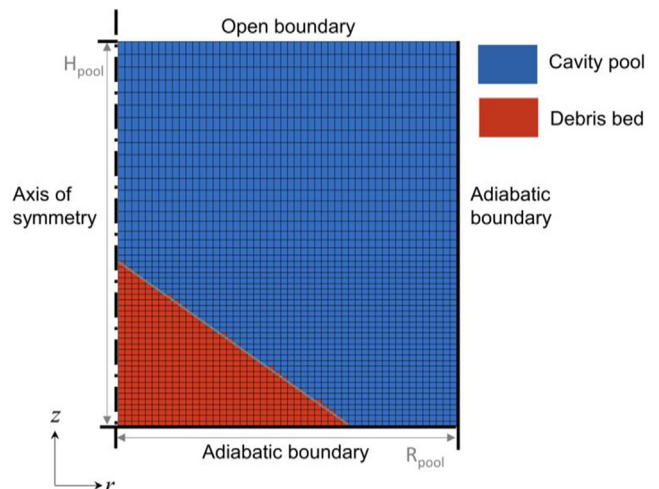


Fig. 6. Computational domain of COCOMO code.

reactor scram in Fig. 7. The decay power of the debris bed in cavity only includes the part that is generated by the unreleased fission products. It is lower than the total decay power curve because part of the radioactive fission products is released with aerosols or dissolved in the pool.

Many previous investigations assume a uniform definition of initial bed temperature. For instance, 1273 K is used for a prototypical debris bed of a reference Nordic-type BWR with thermal power of 2100 MW (Huang and Ma, 2018a). Besides, in a simulation study of jet release in a BWR scenario, the average temperature of the settled particles is between 1500 K and 1700 K (Rahman, 2013). In the present study, the initial debris bed temperature is estimated based on the MELCOR prediction. From MELCOR data output, the total energy of all corium, the energy loss during corium release and the mass of each composition can be obtained directly as a variance of time. The initial bed temperature is treated as the temperature of all corium, averaged from the total energy at the vessel failure time minus the energy loss during corium settling as predicted by FDI package. As a result, the initial temperature is 1854 K.

It should be noted that the calculation of initial temperature is based on the assumption that all corium is released to the cavity immediately at vessel failure time. However, in MELCOR simulation, the corium release process is in 30 min. This means in the coupled simulation, extra energy is introduced to the system, due to the co-exist of unreleased corium inside vessel in MELCOR and the debris bed in COCOMO during the corium release time. This is the limitation of our current simulation tool. The current simulation is conservative.

Other debris bed properties such as the particle size, the shape of debris bed, and the bed porosity are quite uncertain due to the stochastic process of debris bed formation. Our previous study shows that the debris bed coolability is influenced by these properties (Chen and Ma, 2020). They are discussed as following:

The computational models normally treat the particles in the debris bed as spherical. A concept of an effective diameter has been promoted to describe a complex debris bed with only one diameter. It is expected to use the effective diameter of particles in the computational model equations for simplification. Extensive studies have performed but could not find a unified formula due to its complexity. According to previous researches, the Sauter mean diameter (surface-average) is able to represent the effective particle diameter for the pressure drop through a debris bed. While for the dryout prediction of the debris bed, the effective diameter should be lower than the Sauter mean diameter (Chikhi et al., 2014). Some examples for the Sauter mean diameter of debris

simulate material are: 1.75 mm for sand particles used in POMECO-FL tests (Li et al., 2012), and 1.77 mm for irregular gravel ( $\text{Al}_2\text{O}_3$ ) used in COOLOCE tests (Takasuo, 2015). A simulation study shows the Sauter mean diameter of debris bed as a result of BWR jet fragmentation is 1.6 ~ 1.9 mm (Rahman, 2013).

The ex-vessel debris bed is formed as the consequence of the corium jet release and fragmentation, which is a highly complicated and stochastic process. There remain large uncertainties on the final shape of a prototypical debris bed on the cavity floor. The probable shape of the debris bed as a result of a single jet is a heap-like (conical) shape, as observed in DEFOR tests (Karbojian et al., 2009). Moreover, the self-leveling of the debris bed may occur due to the intense boiling of the coolant during the quench process, which reduces the debris bed slope angle (Hilali, 2019).

The theoretical minimum value for the porosity of a homogeneous particulate bed is around 0.36. However, for the ex-vessel debris bed with irregular particles, the porosity would be uncertain. The artificially packed particulate bed is usually compact with small porosity, as measured in experiments e.g. POMECO tests: 0.29 ~ 0.41 (Li et al., 2012), and COOLOCE tests: 0.375 ~ 0.4 (Takasuo, 2016). In jet fragmentation experiments, the porosity is normally larger, e.g. CCM tests: 0.53 ~ 0.68 (Spencer et al., 1994), and DEFOR tests: 0.57 ~ 0.71 (Kudinov et al., 2013). Previous simulation works normally use porosity at around 0.4, e.g. 0.4 in (Rahman, 2013; Takasuo et al., 2015; and Huang and Ma, 2019b), and 0.42 in (Huang and Ma, 2018a) and (Ma and Dinh, 2010).

In order to quantify the effect of mesh volume to the quench simulation by COCOMO code, a test case is simulated with three meshes as listed in Table 3. The debris bed properties of the test case are set with homogenous particle diameter of 2.5 mm, a conical shape with central height of 3 m, and porosity of 0.42. The time for the debris bed to cool to the pool temperature is listed in Table 3. We consider the time difference between mesh No. 2 and 3 is acceptable. Taking the computational efficiency into account, the mesh No.2 is selected in the following simulations.

#### 4.2.2. Effective particle diameter

The particle morphology as the result of melt jet fragmentation observed from CCM tests is major spherical-like, with a typical diameter of 3 mm (Lindholm, 2002). FARO test series show that the particle size is a distribution in the order of millimeter. However, for different test conditions, the measured distributions are not the same (Magallon and Huhtiniemi, 2001). Some relationships could be observed from the experiments, for example, the occurrence of the steam explosion would cause the existence of more small particles.

The COCOMO code allows the definition of the particle diameter with a specific value in each mesh cell. Based on this capability, the effective particle diameter of a debris bed for the quench process is investigated. The distribution of particle size in the present study uses the measurements from FARO test L31. The FARO tests were aimed to investigate the corium jet breakup and fragmentation in a water pool. They were performed with prototypical corium material comprising a mixture of 80%  $\text{UO}_2$  and 20%  $\text{ZrO}_2$ . Different system pressure and pool saturation was tested. The corium melt mass in L31 test was 92 kg. The melt was released into a highly

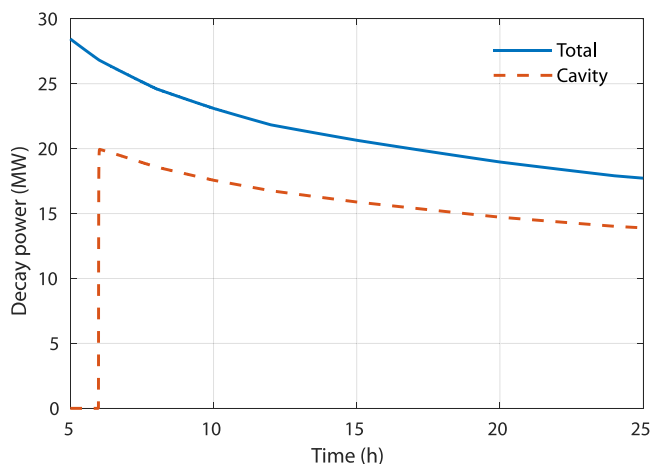


Fig. 7. Total decay power and the decay power of the debris bed in cavity.

Table 3  
Mesh independency test.

Mesh No.	Mesh size	Quench time (s)	Difference
1	50×50	5958.0	–
2	75×75	6384.8	6.68%
3	100×100	6700.4	4.71%

subcooled pool with pool temperature 291 K, and the initial pressure 2.2 bar. It was found in L31 test that all corium was well-fragmented and a particulate debris bed was formed (Magallon and Huhtiniemi, 2001). The test condition of L31 is very similar with the Nordic BWR scenario in the present study. Thus, the distribution of particle size from L31 is considered.

The particles of L31 were separated into three layers for measurement. Each layer was sieved independently. Thus, three distributions of particle size were obtained regarding three layers, as plotted in Fig. 8. The data for the top, middle and bottom distribution are collected from (Lindholm, 2002). The data for the total distribution are collected from (Magallon and Huhtiniemi, 2001). A rough estimation indicates that three layers were probably equal in mass. A stratification can be found that the top layer has higher proportion of small particles, while the bottom layer has relatively lower proportion of small particles.

The computational domain of COCOMO is shown in Fig. 9, with the axis of symmetry on the left boundary. The shape of debris bed is considered to be conical, which is likely as the result of the single jet release from the central bottom of the vessel. There are no clear evidences on the critical angle of repose for particulate debris. In a previous study on the particulate debris phenomenon effect, an uncertainty is considered for the critical angle of repose within the range of (22°, 35°); see (Basso et al., 2016). The maximum limit value is adopted as the slope angle in our simulation, which is 35°. The bed porosity is assumed as 0.42.

Each layer is defined with a particle size profile, which is sampled from the corresponding particle size distribution in Fig. 8. In order to reduce the sampling error, the sampling is performed multiple times. There are several definitions of mean diameter for particles with inhomogeneous size. For spherical particles, four definitions are listed in Table 4. The Sauter mean diameter as mentioned above is the surface mean diameter. The mean diameter ranges for the sampled cases are also listed in the Table 4.

The coupled simulation is performed for all these sampled cases. As representative, the case with the maximum mean particle diameter is selected to show the temperature distributions at different time, in Fig. 10. The debris bed surface is marked with a solid grey line in each plot. The coolant velocity vector is marked with white dotted arrows for gas phase, and green solid arrows for liquid phase. With the liquid coolant penetration into the bed from the surface, water is heated into steam in the hot bed. The steam flows upwards and exits from the top of the bed. The natural circulation is formed in the pool. The hot debris bed (in red) is quenched gradually, and the quench front propagates from the surface near bottom to the central top of the bed.

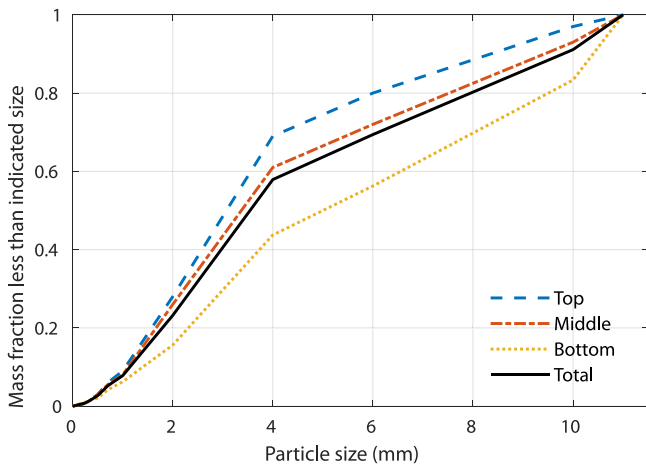


Fig. 8. FARO L31 test particle size distribution.

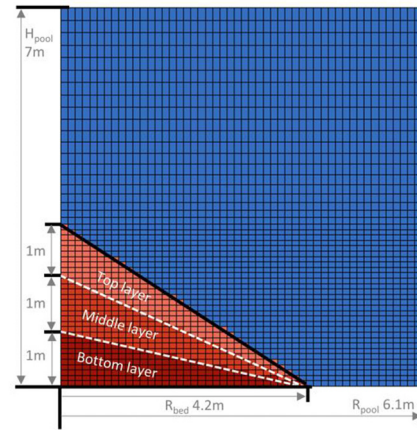


Fig. 9. Computational domain of the debris bed in cavity pool.

Table 4

Definitions of mean diameter for spherical particles with inhomogeneous size.

Symbol	Name	Expression	Sampling from L31 distribution
$d_n$	Count mean diameter	$\frac{\sum n_i d_i}{\sum n_i}$	0.37 ~ 0.54 mm
$d_l$	Length mean diameter	$\frac{\sum n_i d_i^2}{\sum n_i d_i}$	0.73 ~ 1.09 mm
$d_s$	Surface mean diameter	$\frac{\sum n_i d_i^3}{\sum n_i d_i^2}$	2.07 ~ 2.51 mm
$d_v$	Volume mean diameter	$\frac{\sum n_i d_i^4}{\sum n_i d_i^3}$	4.36 ~ 4.80 mm

Fig. 11 shows the quenched bed mass fraction with time, for two sampled cases with inhomogeneous particle size plotted in blue solid lines: (a) the case with the maximum mean diameter; and (b) the case with the minimum mean diameter. In each plot, the result is compared with the scenario when the debris bed is defined with homogenous particle size: the red dash-dotted line representing the homogenous particle diameter defined as the Sauter mean diameter of the inhomogeneous case, and the black dashed line representing the homogenous particle diameter defined as 1.1 times the Sauter mean diameter of the inhomogeneous case. The lines in the figure are similar to logarithm function, which indicates a gradual decrease of quench rate with time. The black dashed lines are on the left side of red dash-dotted lines, which shows that the homogenous bed with larger particle diameter is quenched faster. It is because the larger particle diameter leads to smaller friction, which promotes the coolant flow penetration inside the debris bed. The sampled cases with inhomogeneous diameter (blue solid lines) are more close to the black dashed lines. Therefore, if one diameter is used to describe the inhomogeneous case regarding the quenched mass fraction, the effective particle diameter would be suggested larger than the Sauter mean diameter, to be more precise, approximately 10% larger than the Sauter mean diameter according to the simulation.

In order to quantify the local temperature increase, the maximum temperature and the fraction of bed mass with certain temperature increases are listed in Table 5. Two homogenous cases are also listed as comparison, which are the 1.1 times the maximum and minimum Sauter mean diameter, also used in Fig. 11. The inhomogeneous cases generally have approximately one third of the bed with temperature increase over 100 K, and less than 5% of the bed with temperature increase over 400 K.

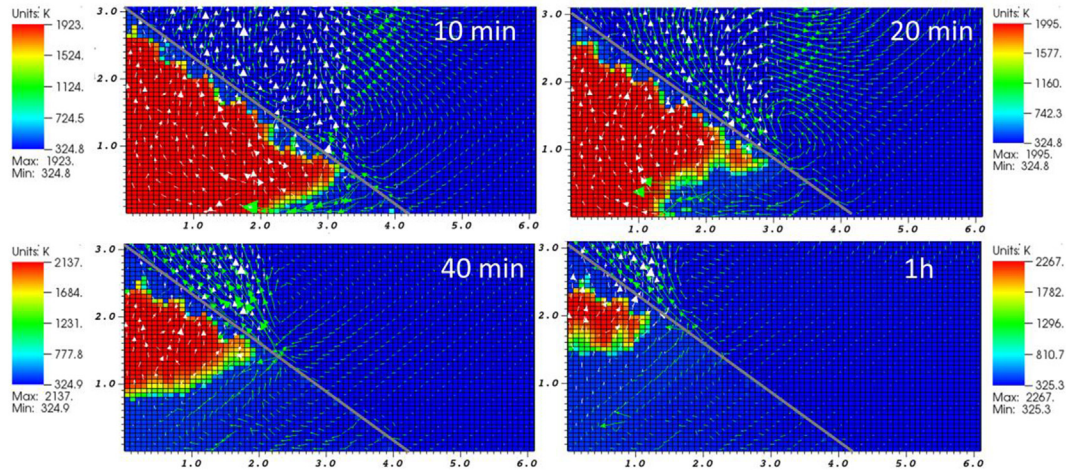


Fig. 10. Temperature distribution of the debris bed during quench.

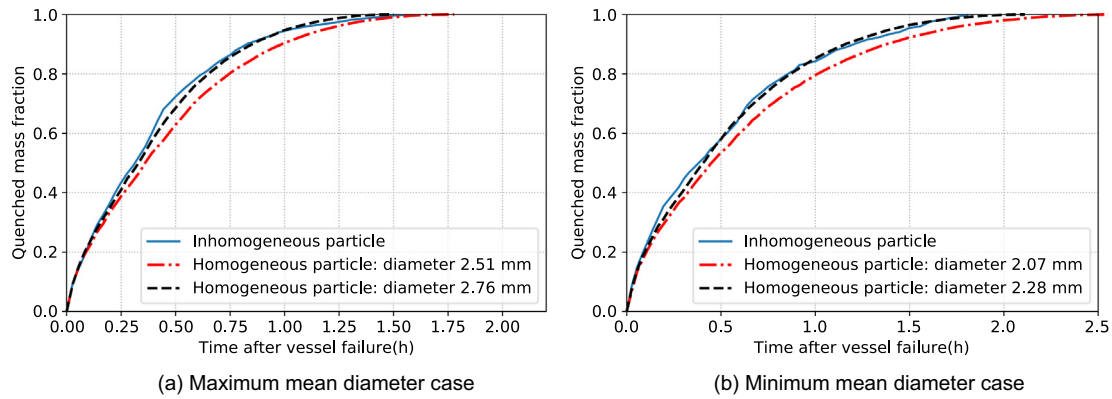


Fig. 11. Quenched mass fraction with time.

The homogenous case with particle diameter of 2.76 mm is within the inhomogeneous case range, while the 2.28 mm case is higher than the range. It means the 2.28 mm case predicts a more severe situation than any of the inhomogeneous cases. The result indicates that the effective particle diameter using 10% larger than the Sauter mean diameter would be conservative enough to represent the variance of bed maximum temperature with time.

#### 4.2.3. Effect of debris bed shape

Considering the uncertainty on the shape of debris bed, and the possible self-leveling of the debris bed, three scenarios of bed shapes are discussed. Fig. 12 shows the computational domain of these three scenarios. Case A is the same in previous discussion. Case B has a smaller slope angle, which is the minimum limit of critical repose angle uncertainty considered in (Basso et al., 2016). Case C is an ideal and extreme assumption that all particles fully cover the entire cavity floor with the same thickness of the

bed. The debris beds in three cases are assumed to be homogenous with porosity 0.42. The effective diameter is selected as the middle value of the two homogenous cases in Table 5, which is considered to be 2.5 mm.

The temperature distribution for three cases is shown in Figs. 13–15. Case A and B have similar quench front propagation, also similar with the inhomogeneous case in Fig. 10. Case C is quite different. The one-dimensional quench front is observed along the axial direction from the top of the bed to the bottom. The velocity of coolant is generally in 1D. The downward liquid flow is hindered by the upward steam flow. The flat and homogenous debris bed like case C is also called 1D debris bed. Correspondingly, the conical debris bed e.g. case A and B are 2D debris beds, due to the 2D coolant flow pattern.

The maximum temperature of the debris bed occurs at the place where the liquid coolant could penetrate last. For 2D beds, the maximum temperature is located on the central top of the bed. While for 1D bed, the maximum temperature is located at the

Table 5

Maximum temperature and mass fraction of debris bed with certain temperature increases.

Case		Homogenous 2.76 mm	Homogenous 2.28 mm	Inhomogeneous cases
Maximum temperature increase		505 K	684 K	429 ~ 581 K
Mass fraction of debris bed with temperature increase	100 K	33.4%	39.5%	29.3%~37.9%
	200 K	14.5%	20.9%	10.9%~18.9%
	300 K	5.2%	10.9%	3.6%~8.0%
	400 K	1.1%	4.9%	0.3% ~ 2.3%

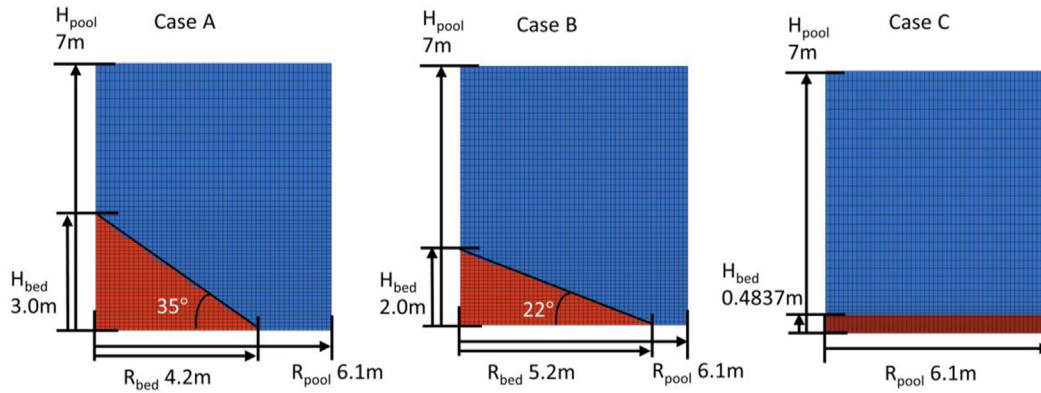


Fig. 12. The computational domains for three cases with different bed shapes.

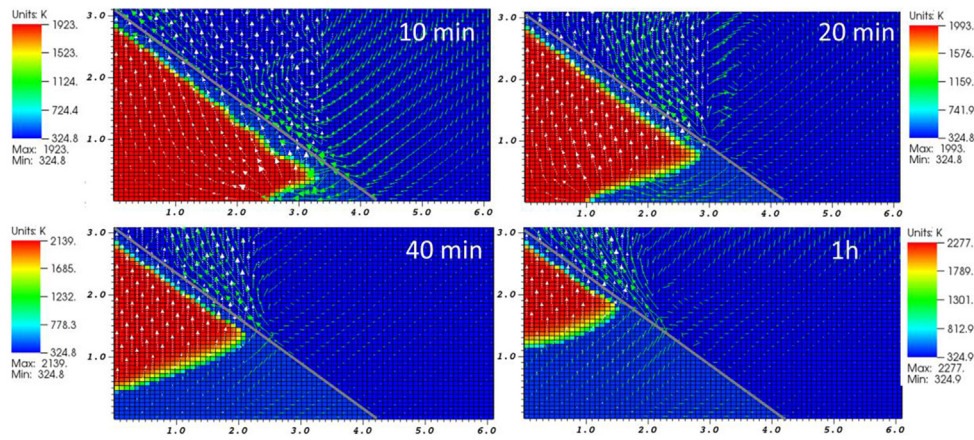


Fig. 13. Temperature distribution for Case A.

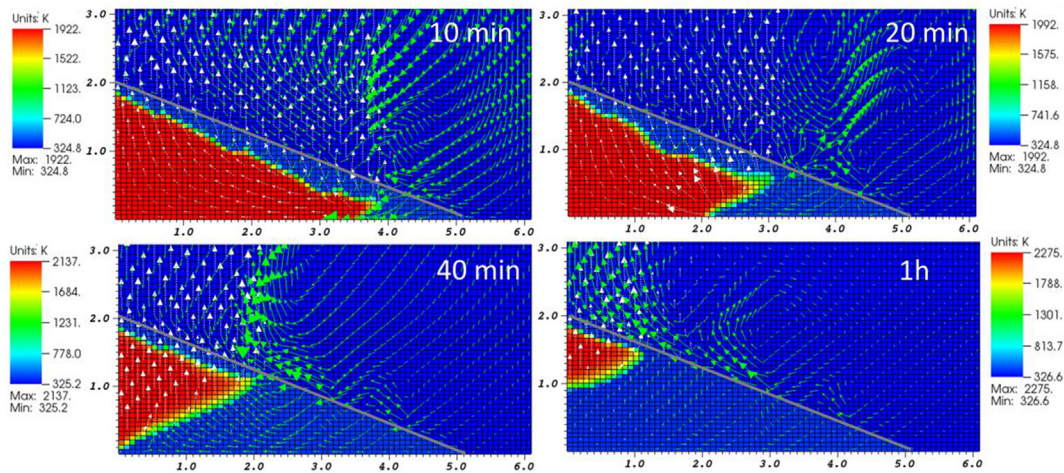


Fig. 14. Temperature distribution for Case B.

bottom layer. The maximum temperature of the debris bed is plotted as a variance of time in Fig. 16. The same temperature increase is found at around the first quarter. Then Case C is fully quenched. The debris bed with larger slope angle (Case A) tends to take longer time to quench. Fig. 17 shows the mass fraction of the debris bed with a temperature increase higher than the corresponding x-axis value. Although the maximum temperature for Case A, B and C reaches 2446 K (592 K increase), 2315 K (461 K increase), and

1961 K (107 K increase), there is only very small portion of debris bed that could reach that value of temperature. Less than 3% mass has the temperature increase of 400 K for Case A, and 300 K for Case B.

The mass fraction of quenched debris bed is plotted in Fig. 18. Compared with Case A and B, Case C has a relatively faster quench rate. There seems to be a linear relationship between the quenched mass fraction and the time for case C, due to its 1D quench front

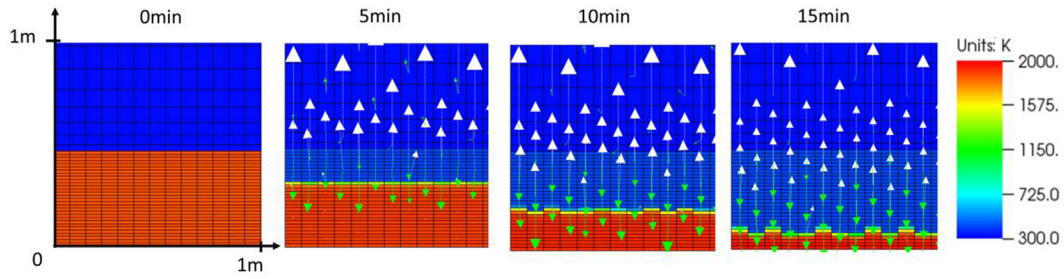


Fig. 15. Temperature distribution for Case C.

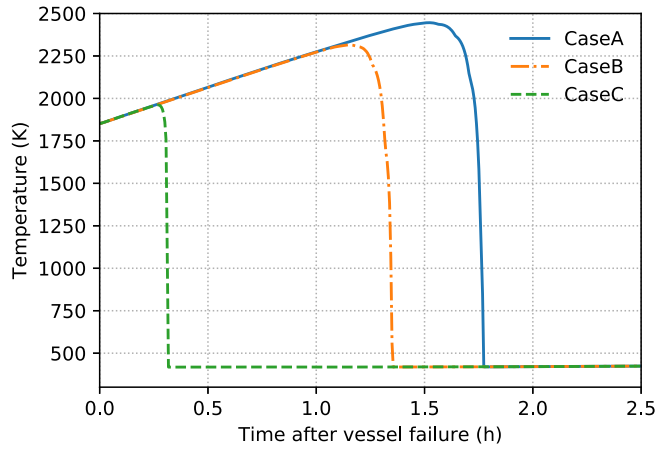


Fig. 16. Bed maximum temperature for Case A, B and C.

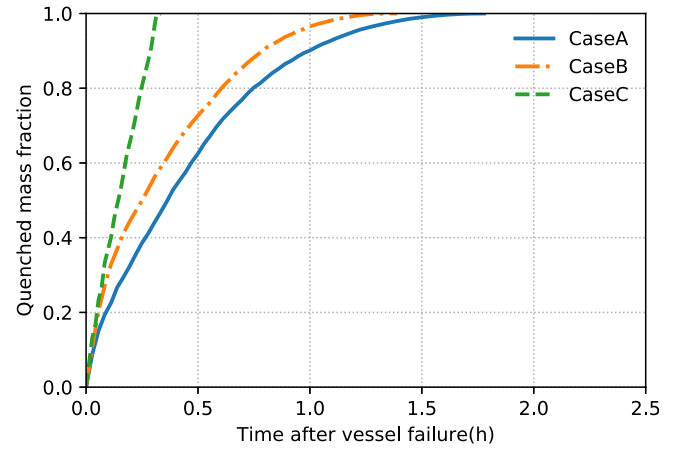


Fig. 18. Mass fraction of quenched debris bed with time for Case A, B and C.

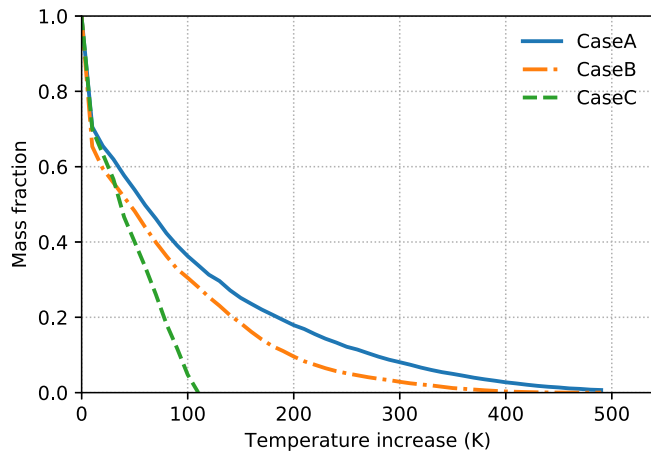


Fig. 17. Mass fraction of the debris bed with the temperature increase for Case A, B and C.

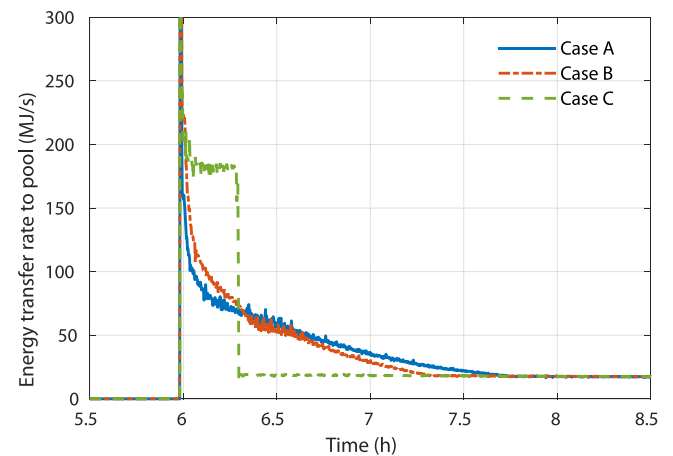


Fig. 19. Energy transfer rate from debris bed to cavity pool for Case A, B and C.

propagation. Based on above observations, there is a trend that with the decrease of bed slope angle (from Case A to C), it takes less time to quench and has lower temperature increase. Therefore, the self-leveling would promote the debris bed quench. Our simulation without the consideration of debris bed self-leveling would be conservative.

The energy transfer rate from debris bed to the pool calculated by COCOMO is provided to MELCOR as the energy source of the cavity pool. The total energy of the debris bed to be removed by the pool is the same for all three cases, since they have the same initial temperature and decay power. However, the energy transfer rate is quite different as plotted in Fig. 19. The energy transfer rate of 2D beds (Case A and B) gradually decreases and approaches the

decay power. While 1D bed (Case C) keeps at higher energy transfer rate at the beginning than other two cases. Then, the energy transfer rate suddenly drops to the decay power level when 1D bed is fully quenched.

The containment pressure calculated by MELCOR is plotted in Fig. 20, including three coupled simulation cases and the MELCOR standalone case. After vessel failure, the highly subcooled cavity pool is heated with the energy from COCOMO in the coupled simulation, or from the CAV package in MELCOR standalone simulation. After the pool is saturated, the containment pressure increases fast due to the steam generated from the pool. The containment venting is triggered when the pressure reaches the critical value, and then pressure drops. Among the coupled simulations, only minor differences can be found. Compared with

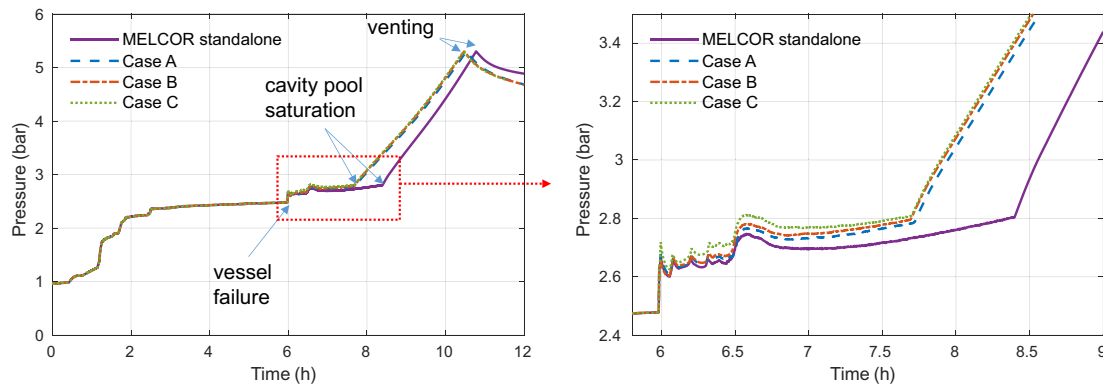


Fig. 20. Containment pressure for MELCOR standalone and coupled cases.

the coupled simulations, MELCOR standalone simulation predicts a later time to reach the cavity pool saturation and the containment venting. Coupled simulations predict the debris beds are fully quenched to the pool temperature in around one hours. While the MELCOR standalone simulation predicts that the debris in CAV package is still at high temperature of 1000 K at 10 h after vessel failure. There is faster energy transferred from the debris bed to the pool in the coupled simulations, and thus it promotes the faster pressure transient.

## 5. Conclusions

The coupling of MELCOR and COCOMO is developed to extend the MELCOR capability for analysis of ex-vessel debris bed coolability, in order to satisfy the contemporary need on the analysis of quenching process for ex-vessel debris beds formed in postulated severe accidents of Nordic BWR. In the coupling approach, the COCOMO code is employed to simulate the thermal-hydraulics of a debris bed in the cavity, while MELCOR is used to simulate the accident progression and response in the entire reactor system.

The station blackout (SBO) scenario is considered as the initiating event of postulated severe accidents in the BWR. In the coupled simulation, the debris bed defined in the COCOMO simulation is based on the specific discharge of mass, composition and temperature of corium into the cavity predicted by the MELCOR simulation. The other properties of the debris bed such as porosity, particle size distribution and bed geometry are given by available data in literature or assumptions. The effects of some bed properties on the quench process are discussed.

A conical inhomogeneous debris bed is assumed to be packed with spherical particulate debris which have the same particle size distribution measured in the FARO L31 test. In the coupled simulation, it is found that the effective particle diameter employed for the prototypical debris bed should be approximately 10% larger than the Sauter mean diameter of the debris particles, in order to have the same mass-averaged quench rate and the maximum temperature increase.

The coupled simulations with varied debris bed configurations indicate that the propagation of quench front is driven by flow patterns inside the debris beds. With a decrease in slope angle of debris bed, the debris bed is quenched faster. The 1D debris bed with zero slope angle reaches the maximum quench rate. Compared with the MELCOR standalone analysis, the coupled simulation predicts earlier points in time to reach the cavity pool saturation and to activate containment venting.

It should be noted that the process of debris bed formation (e.g., settlement of debris particles on the floor of the cavity and

evolution of debris bed geometry) is not captured in current study, although it could be influential to the quench. The possible chemical reactions, e.g., the oxidation of Zr, is also neglected in the present study. Modeling of these phenomena would be the focus of future studies.

## CRediT authorship contribution statement

**Yangli Chen:** Conceptualization, Methodology, Software, Validation, Formal analysis, Investigation, Data curation, Writing – original draft, Visualization. **Huimin Zhang:** Conceptualization, Methodology, Software, Resources. **Weimin Ma:** Resources, Writing – review & editing, Supervision, Project administration, Funding acquisition.

## Declaration of Competing Interest

The authors declare that they have no known competing financial interests or personal relationships that could have appeared to influence the work reported in this paper.

## Acknowledgements

This research work was made possible by the supports of APRI, Swedish Radiation Safety Authority (SSM) and Swiss Federal Nuclear Safety Inspectorate (ENSI). The authors acknowledge the IKE at University of Stuttgart for providing COCOMO code. Special thanks to Dr. Michael Buck for the knowledgeable guidance. The MELCOR code is available to KTH through an agreement between SSM and U.S. NRC. The DINAMO program is developed by Karlsruhe Institute of Technology. The authors are also grateful to the support of the China Scholarship Council.

## References

- Basso, S., Kononenko, A., Yakush, S.E., Kudinov, P., 2016. The effect of self-leveling on debris bed coolability under severe accident conditions. Nucl. Eng. Des. 305, 246–259. <https://doi.org/10.1016/j.nucengdes.2016.05.020>.
- Bürger, M., Buck, M., Schmidt, W., Widmann, W., 2006. Validation and application of the WABE code: Investigations of constitutive laws and 2D effects on debris coolability. Nucl. Eng. Des. 236 (19–21), 2164–2188. <https://doi.org/10.1016/j.nucengdes.2006.03.058>.
- Chen, Y., Ma, W., 2020. Development and application of a surrogate model for quick estimation of ex-vessel debris bed coolability. Nucl. Eng. Des. 370, 110898. <https://doi.org/10.1016/j.nucengdes.2020.110898>.
- Chen, Y., Zhang, H., Villanueva, W., Ma, W., Bechta, S., 2019. A sensitivity study of MELCOR nodalization for simulation of in-vessel severe accident progression in a boiling water reactor. Nucl. Eng. Des. 343, 22–37. <https://doi.org/10.1016/j.nucengdes.2018.12.011>.
- Chikhi, N., Coindreau, O., Li, L.X., Ma, W.M., Taivassalo, V., Takasuo, E., Leininger, S., Kulenovic, R., Laurien, E., 2014. Evaluation of an effective diameter to study

- quenching and dry-out of complex debris bed. *Ann. Nucl. Energy* 74, 24–41. <https://doi.org/10.1016/j.anucene.2014.05.009>.
- Chikhi, N., Fichot, F., 2017. Experimental and theoretical study of large scale debris bed reflood in the PEARL facility. *Nucl. Eng. Des.* 312, 48–58. <https://doi.org/10.1016/j.nucengdes.2016.05.009>.
- Cho, D.H., Armstrong, D.R., Chan, S.H., 1984. On the pattern of penetration into a hot particle bed. *Nucl. Technol.* 65, 23–31. <https://doi.org/10.13182/NT84-A33369>.
- Dietrich, P., 2016. *Expansion of the Severe Accident Code MELCOR by Coupling External Models*. KIT Scientific Publishing, Karlsruhe.
- Ergun, S., 1952. Fluid Flow through Packed Columns. *Chem. Eng. Prog.* 48, 89–94.
- Hilali, W., 2019. *Debris Bed Formation in Degraded Cores of Light Water Reactors*. Universität Stuttgart. <https://doi.org/http://dx.doi.org/10.18419/opus-10296>.
- Hu, K., Theofanous, T.G., 1991. On the measurement and mechanism of dryout in volumetrically heated coarse particle beds. *Int. J. Multiph. Flow* 17 (4), 519–532. [https://doi.org/10.1016/0301-9322\(91\)90047-7](https://doi.org/10.1016/0301-9322(91)90047-7).
- Huang, Z., Ma, W., 2019a. On the quench of a debris bed in the lower head of a Nordic BWR by coolant injection through control rod guide tubes. *Nucl. Eng. Des.* 351, 189–202. <https://doi.org/10.1016/j.nucengdes.2019.06.001>.
- Huang, Z., Ma, W., 2019b. Performance of a passive cooling system for spent fuel pool using two-phase thermosiphon evaluated by RELAP5/MELCOR coupling analysis. *Ann. Nucl. Energy* 128, 330–340. <https://doi.org/10.1016/j.anucene.2019.01.024>.
- Huang, Z., Ma, W., 2018a. Validation and application of the MEWA code to analysis of debris bed coolability. *Nucl. Eng. Des.* 327, 22–37. <https://doi.org/10.1016/j.nucengdes.2017.11.038>.
- Huang, Z., Ma, W., 2018b. Numerical investigation on quench of an ex-vessel debris bed at prototypical scale. *Ann. Nucl. Energy* 122, 47–61. <https://doi.org/10.1016/j.anucene.2018.08.018>.
- Humphries, L.L., Beeny, B.A., Gelbard, F., Louie, D.L., Phillips, J., 2017. *MELCOR Computer Code Manuals Vol.2: Reference Manual*. Albuquerque, NM 87185-0748.
- Karbojian, A., Ma, W.M., Kudinov, P., Dinh, T.N., 2009. A scoping study of debris bed formation in the DEFOR test facility 239 (9), 1653–1659. <https://doi.org/10.1016/j.nucengdes.2009.03.002>.
- Kudinov, P., Karbojian, A., Tran, C.T., Villanueva, W., 2013. Agglomeration and size distribution of debris in DEFOR-A experiments with Bi2O3-WO3 corium simulat melt. *Nucl. Eng. Des.* 263, 284–295. <https://doi.org/10.1016/j.nucengdes.2013.06.011>.
- Li, L., Ma, W., Thakre, S., 2012. An experimental study on pressure drop and dryout heat flux of two-phase flow in packed beds of multi-sized and irregular particles. *Nucl. Eng. Des.* 242, 369–378. <https://doi.org/10.1016/j.nucengdes.2011.11.006>.
- Lindholm, I., 2002. *A Review of Dryout Heat Fluxes and Coolability of Particle Beds*. SKI report 02, 17.
- Lipinski, R.J., 1982. *A Model for Boiling and Dryout in Particle Beds*. Sandia National Laboratories. Sandia National Laboratories, NUREG/CR-2646 SAND82-0765.
- Ma, W., Dinh, T., 2010. The effects of debris bed 's prototypical characteristics on corium coolability in a LWR severe accident 240, 598–608. <https://doi.org/10.1016/j.nucengdes.2009.10.026>.
- Magallon, D., Huhtiniemi, I., 2001. Corium melt quenching tests at low pressure and subcooled water in FARO 204, 369–376.
- Mohsen Hoseyni, S., Villanueva, W., Thakre, S., Konovalenko, A., Bechta, S., 2021. Melt infiltration through porous debris at temperatures above Solidification: Validation of analytical model. *Ann. Nucl. Energy* 161, 108435. <https://doi.org/10.1016/j.anucene.2021.108435>.
- Rahman, S., 2013. *Coolability of Corium Debris under Severe Accident Conditions in Light Water Reactors*. Universität Stuttgart. <https://doi.org/http://dx.doi.org/10.18419/opus-2168>.
- Reed, A.W., 1982. *The effect of channeling on the dryout of heated particulate beds immersed in a liquid pool* (Ph.D Thesis). Massachusetts Institute of Technology, Cambridge, USA.
- Schäfer, P., Groll, M., Kulenovic, R., 2006. Basic investigations on debris cooling. *Nucl. Eng. Des.* 236 (19–21), 2104–2116. <https://doi.org/10.1016/j.nucengdes.2006.03.033>.
- Schulenberg, T., Müller, U., 1986. *A refined model for the coolability of core debris with flow entry from the bottom*. University of California, Los Angeles.
- Spencer, B.W., Wang, K., Blomquist, C.A., McUmber, L.M., Schneider, J.P., 1994. *Fragmentation and quench behavior of corium melt streams in water*. NUREG/CR-6133, ANL-93/32, Nuclear Regulatory Commission, Washington, DC, USA.
- Szabó, T., Kretzschmar, F., Schulenberg, T., 2014. Obtaining a more realistic hydrogen distribution in the containment by coupling MELCOR with GASFLOW. *Nucl. Eng. Des.* 269, 330–339. <https://doi.org/10.1016/j.nucengdes.2013.07.009>.
- Takasuo, E., 2016. *A summary of studies on debris bed coolability and multi-dimensional flooding*. NKS-374 ISBN 978-87-7893-459-8, VTT Technical Research Centre of Finland Ltd.
- Takasuo, E., 2015. *Coolability of porous core debris beds Effects of bed geometry and multi- Coolability of porous core debris beds* (Ph.D thesis). VTT Technical Research Centre of Finland Ltd.
- Takasuo, E., Holmström, S., Kinnunen, T., Pankakoski, P.H., 2012. The COOLOCE experiments investigating the dryout power in debris beds of heap-like and cylindrical geometries. *Nucl. Eng. Des.* 250, 687–700. <https://doi.org/10.1016/j.nucengdes.2012.06.015>.
- Takasuo, E., Taivassalo, V., Kinnunen, T., Lehtikuus, T., 2015. Coolability analyses of heap-shaped debris bed. NKS-343.
- Thakre, S., Li, L., Ma, W., 2014. An experimental study on coolability of a particulate bed with radial stratification or triangular shape. *Nucl. Eng. Des.* 276, 54–63. <https://doi.org/10.1016/j.nucengdes.2014.04.039>.
- Tung, V.X., Dhir, V.K., 1988. A hydrodynamic model for two-phase flow through porous media. *Int. J. Multiph. Flow* 14 (1), 47–65. [https://doi.org/10.1016/0301-9322\(88\)90033-X](https://doi.org/10.1016/0301-9322(88)90033-X).
- Tung, V.X., Dhir, V.K., 1987. Quenching of debris beds having variable permeability in the axial and radial directions. *Nucl. Eng. Des.* 99, 275–284. [https://doi.org/10.1016/0029-5493\(87\)90127-0](https://doi.org/10.1016/0029-5493(87)90127-0).
- Tutu, N.K., Ginsberg, T., Klein, J., Klages, J., Schwarz, C.E., 1984. *Debris bed quenching under bottom flood conditions (in-vessel degraded core cooling phenomenology)*. NUREG/CR-3850, United States.
- Yakush, S.E., Kudinov, P., 2016. *In-Vessel Debris Bed Coolability and Implications For Vessel Failure Mode*. The 11th International Topical Meeting on Nuclear Thermal-Hydraulics, Operation and Safety (NUTHOS-11).
- Yakush, S.E., Kudinov, P., Villanueva, W., Basso, S., 2013. In-Vessel Debris Bed Coolability and its Influence on the Vessel Failure, in: 15th International Topical Meeting on Nuclear Reactor Thermal Hydraulics (NURETH15). Pisa, Italy.
- Yakush, S.E., Villanueva, W., Basso, S., Kudinov, P., 2014. Simulation of In-vessel Debris Bed Coolability and Remelting. The 10th International Topical Meeting on Nuclear Thermal-Hydraulics, Operation and Safety (NUTHOS-10), Okinawa, Japan.
- Young, M.F., Murata, K.K., Romero, V.J., Gauntt, R.O., Rochau, G.E., 2004. *Advanced Nuclear Energy Analysis Technology*. Sandia National Laboratories (SNL), SAND 2004-2124, Tech. Rep.